SUPPORTING INFORMATION FOR:

Towards multiple conductance pathways with heterocycle-based oligo(phenyleneethynylene) derivatives

Delia Miguel,[a,*] Luis Álvarez de Cienfuegos,[a] Ana Martín-Lasanta,[a] Sara P. Morcillo,[a] Linda A. Zotti,[b] Edmund Leary,[c] Marius Bürkle,[d] Yoshihiro Asai,[d] Rocío Jurado,[a] Diego J. Cárdenas,[e] Gabino Rubio-Bollinger,[f,g] Nicolás Agraït,[c,f,g] Juan M. Cuerva, [a,*] M. Teresa González [c,*]

[a] Departamento de Química Orgánica, C. U. Fuentenueva, Avda. Severo Ochoa s/n E-18071, Universidad de Granada, Spain.

[b] Departamento of Física Teórica de la Materia Condensada, Universidad Autónoma de Madrid, Ciudad Universitaria de Cantoblanco, E-28049 Madrid, Spain.

[c] Fundación IMDEA Nanociencia, Ciudad Universitaria de Cantoblanco, E-28049, Madrid, Spain.

[d] Nanomaterials Research Institute, National Institute of Advanced Industrial Science and Technology (AIST), Tsukuba, Ibaraki 305-8568, Japan.

[e] Departamento de Química Orgánica, Universidad Autónoma de Madrid, Ciudad Universitaria de Cantoblanco, E-28049, Madrid, Spain.

[f] Departamento de Física de la Materia Condensada and Condensed Matter Physics Center (IFIMAC), Universidad Autónoma de Madrid, E-28049 Madrid, Spain.

[g] Instituto "Nicolás Cabrera" , Universidad Autónoma de Madrid, Ciudad Universitaria de Cantoblanco, E-28049, Madrid, Spain.

Index

Synthesis part. GENERAL INFORMATION

All Sonogashira coupling reactions were assembled under argon atmosphere in oven-dried glassware with magnetic stirring. All commercially available reagents and solvents used in reactions, extractions and purifications (dichlorometane, Et_3N, $^iPr_2NH$, hexane and ethyl acetate) were obtained from standard chemical suppliers and used without further purification. TLC was performed on aluminium-backed plates coated with silica gel 60 (230-240 mesh) with F254 indicator. The spots were visualized with UV light (254 nm) and/or staining with Ce/Mo reagent or phosphomolybdic acid solution and subsequent heating. Column chromatography was carried out using 40-60 μm mesh silica.

NMR Spectra were measured at room temperature. ^1H NMR spectra were recorded at 300, 401 or 500 MHz. Chemical shifts are reported in ppm using residual solvent peak as reference ($CHCl_3$: δ 7.26, CH_2Cl_2 δ 5.30). Data are reported as follows: chemical shift, multiplicity (s: singlet, d: doublet, t: triplet, m: multiplet, dd: doublet of doublets, dt: doublet of triplets, dq: doublet of quartets, td: triplet of doublets), coupling constant (*J* in Hz) and integration. ^{13}C-NMR spectra were recorded at 75.4, 101 or 126 MHz using broadband proton decoupling and chemical shifts are reported in ppm using residual solvent peaks as reference ($CDCl_3$: δ 77.16; CD_2Cl_2 δ 53.52). Carbon multiplicities were assigned by DEPT techniques.

High resolution mass spectra (HRMS) were recorded on a Micromass AutoSpec using EI at 70 eV.

SYNTHETIC PROCEDURES

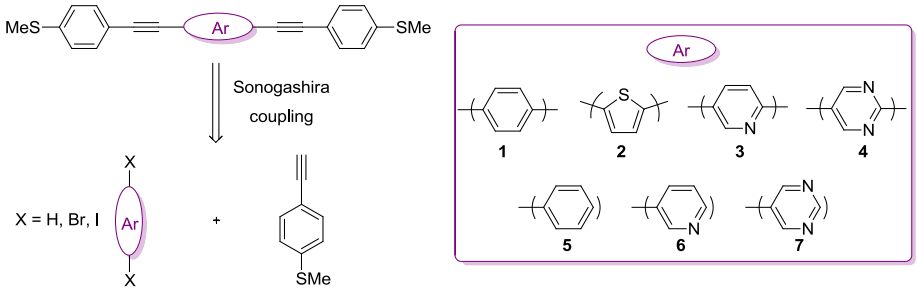

Scheme S1. Retrosynthetic analysis of compounds **1**-**7**.

General procedure for the Sonogashira coupling of aryl iodides (GP 1). A solution of 4-ethynylphenyl methyl sulphide (2.2 mmol for compound **1**, 1.1 mmol for

compounds **5** and **6**) dissolved in the minimum volume of THF and Et_3N was added to a degassed suspension of the corresponding mono- or diiodinated compound (1 mmol), $Pd(PPh_3)_2Cl_2$ (0.05 mmol) and CuI (0.1mmol) in (5 mL) of Et_3N. The reaction was stirred between 3-16h under argon atmosphere at 55 °C for compound 1 and at room temperature for derivatives **5** and **6**. The mixture was then diluted with CH_2Cl_2, washed with saturated aq NH_4Cl solution, dried over Na_2SO_4 and the solvent was removed under reduced pressure. The residue was purified by column chromatography (EtOAc/hexane mixtures) to give the corresponding products that were characterized by ^{1}H-RMN, ^{13}C-RMN and high-resolution mass spectrometry. Known compounds **5**[1] and **6**[2] were isolated as pure sample and showed NMR spectra identical to reported data.

General procedure for Sonogashira coupling of aryl bromides (GP 2). A solution of 4-ethynylphenyl methyl sulphide (2.2 mmol for compound **2**-**4**, 1.1 mmol for compound **7**) dissolved in the minimum volume of THF and iPr_2NH was added to a degassed suspension of the corresponding mono- or dibrominated compound (1 mmol), $Pd(CH_3CN)_2Cl_2$ (0.03mmol), CuI (0.03mmol) and $PtBu_3{\cdot}HBF_4$ (0.06 mmol) in (5 mL) of iPr_2NH. The reaction was stirred between 3-16h under argon atmosphere at 55 °C for compounds **2**-**4** and at room temperature for compound **7**. The mixture was then diluted with CH_2Cl_2, washed with saturated aq NH_4Cl solution, dried over Na_2SO_4 and the solvent was removed under reduced pressure. The residue was purified by column chromatography (EtOAc/hexane mixtures) to give the corresponding products that were characterized by ^{1}H-RMN, ^{13}C-RMN and high-resolution mass spectrometry.

[1] Huang, H.; Hong, L.; Jiang, H.; Chen, K. *J. Org. Chem.* **2008**, *73*, 6037-6040.
[2] Chowdhury, M. A.; Dong, Y.; Chen, Q.-H.; Abdellatif, K. R. A.; Knaus, E. E. *Bioorg. Med. Chem.* **2008**, *16*, 1948-1956.

Copies of ^{1}H-NMR and ^{13}C-NMR spectra of new compounds

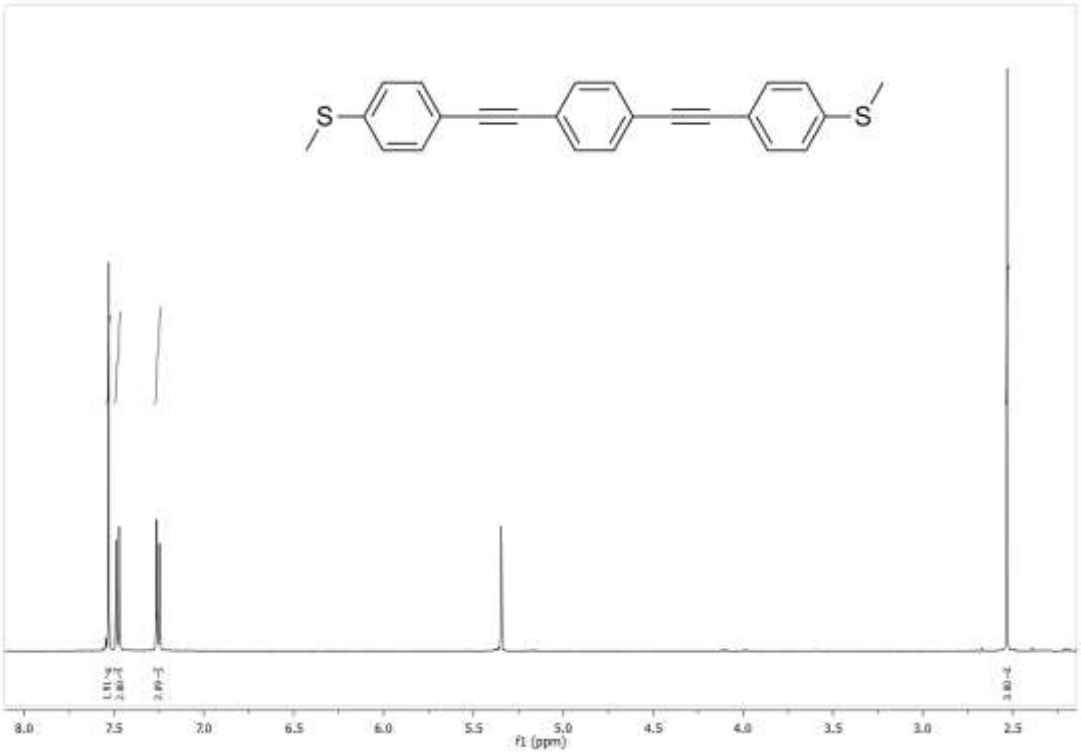

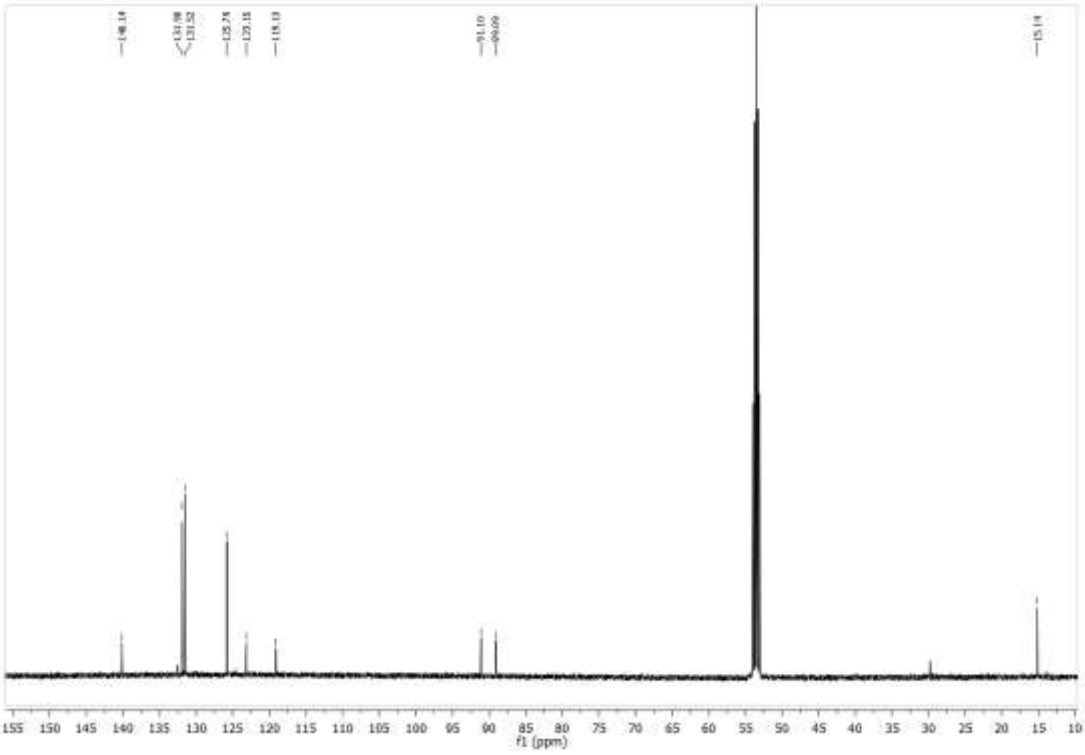

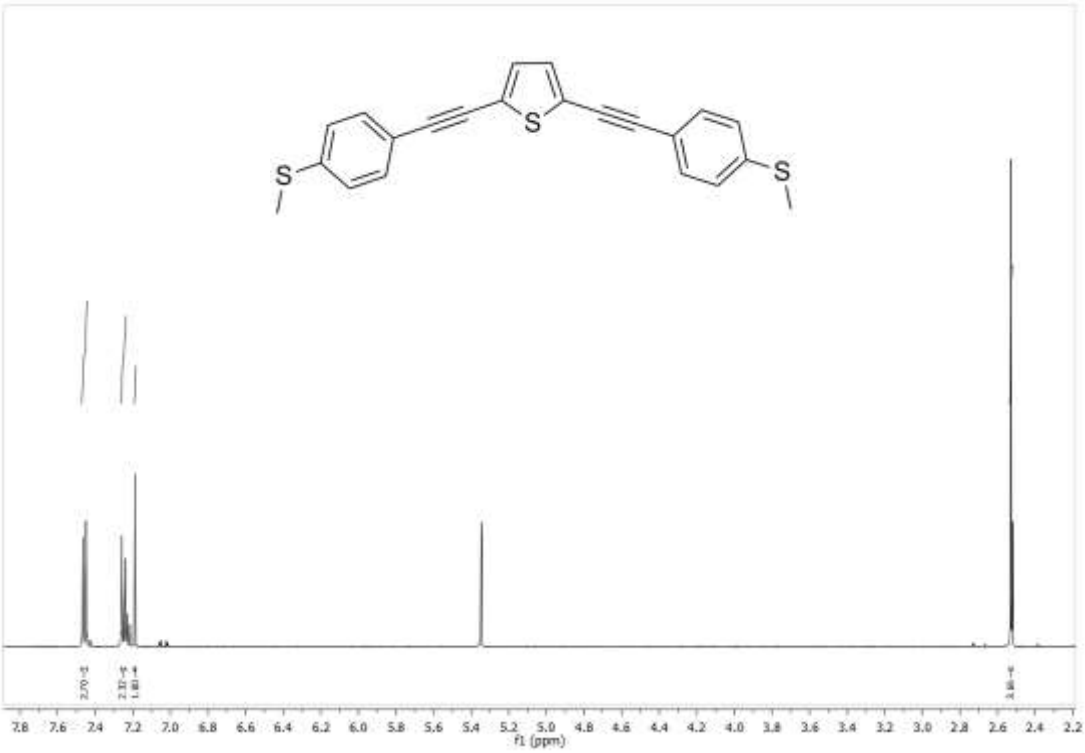
S
S
S
f1 (ppm)

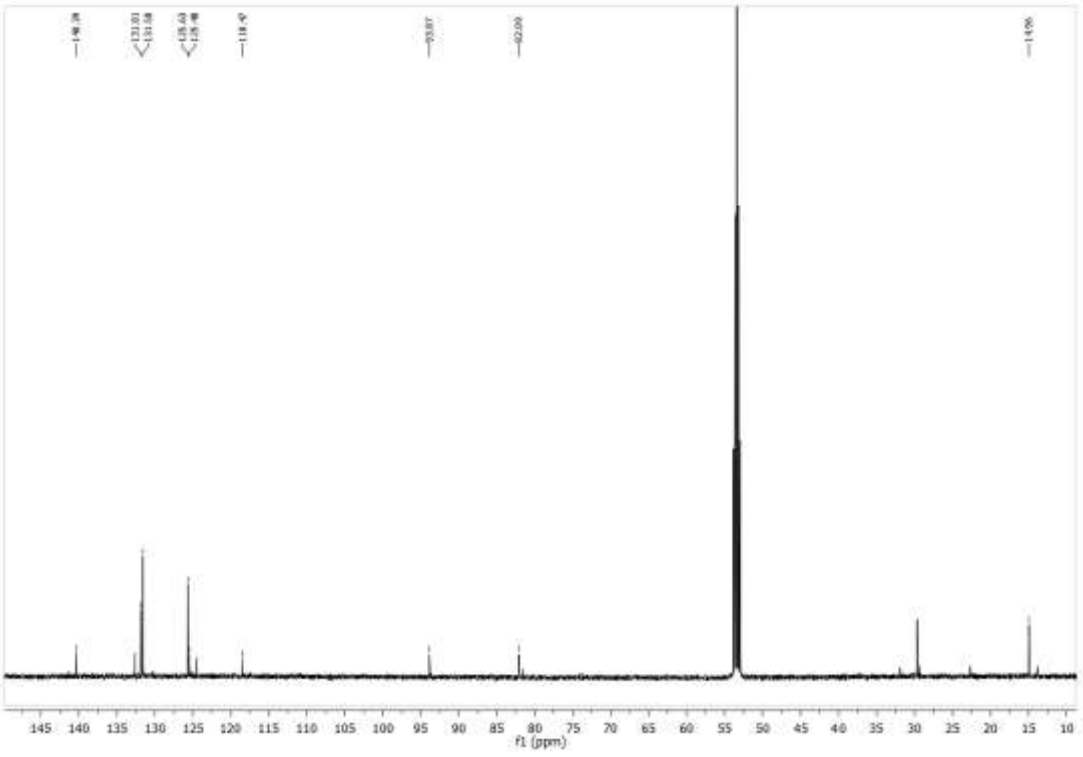
f1 (ppm)

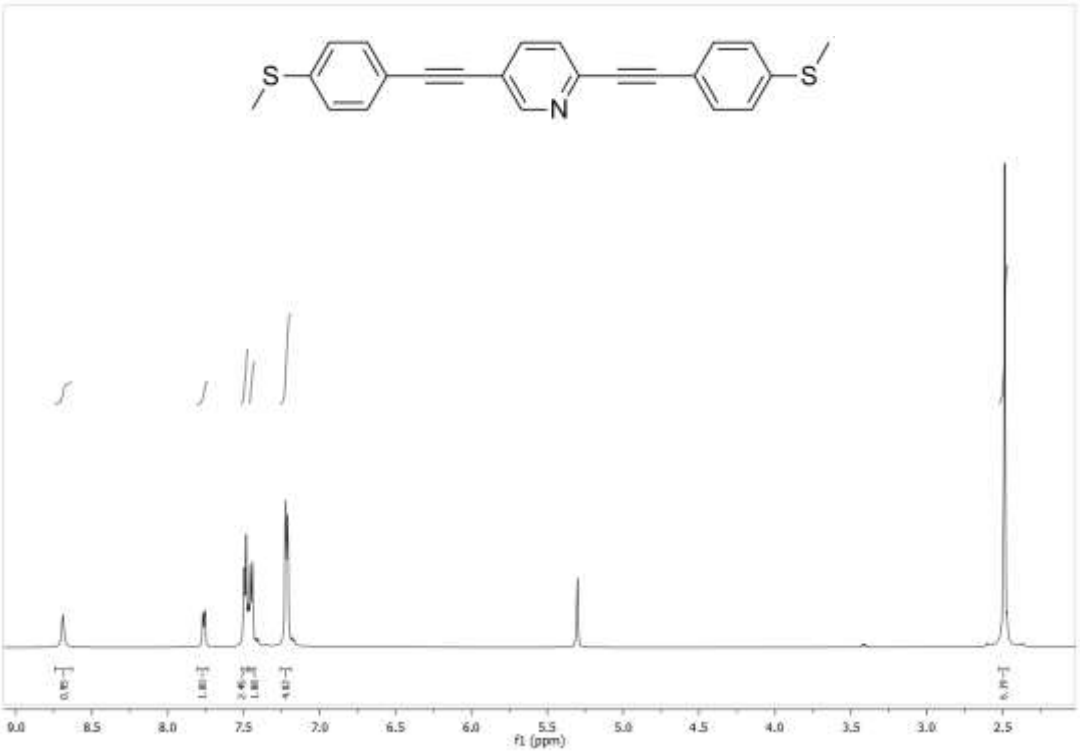
S
N
S
f1 (ppm)

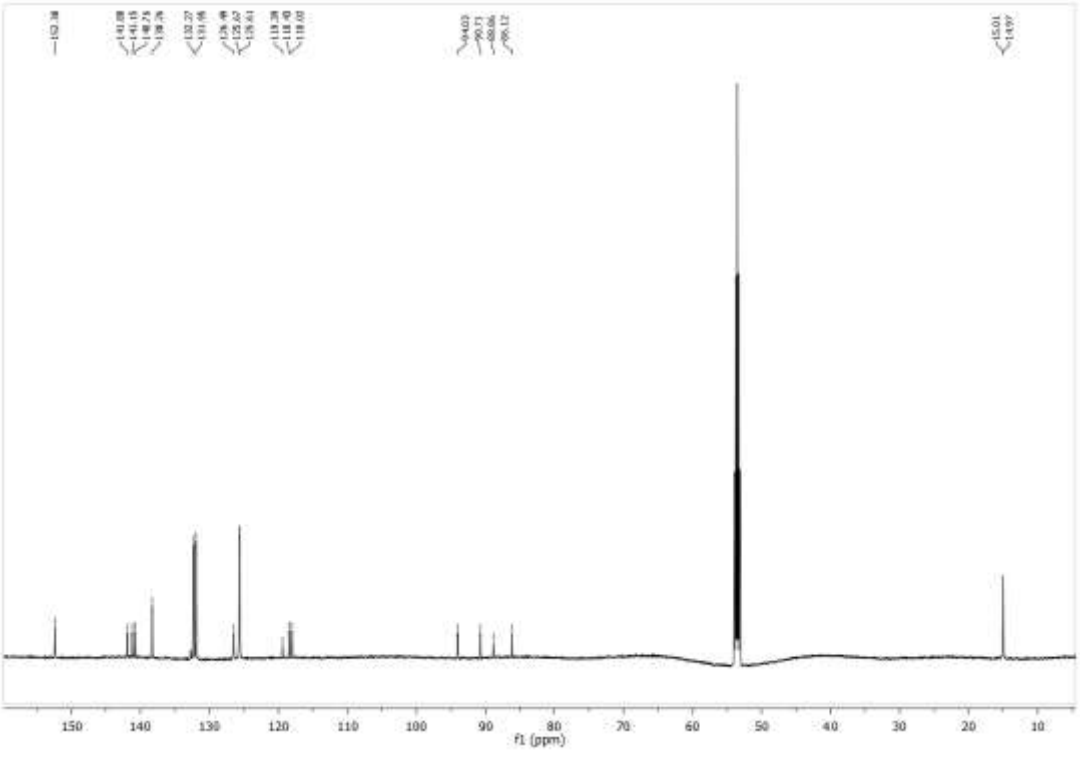
f1 (ppm)

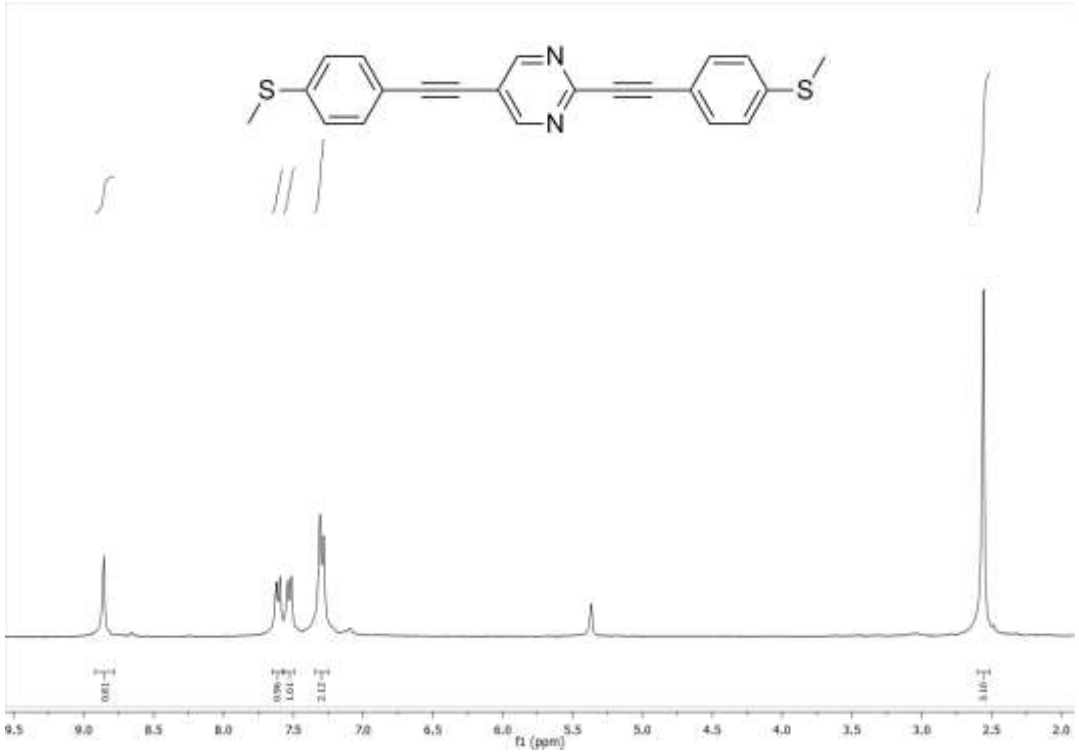
N
N
S
S
0.81
0.96
1.01
2.12
8.10
9.5
9.0
8.5
8.0
7.5
7.0
6.5
6.0
5.5
5.0
4.5
4.0
3.5
3.0
2.5
2.0
f1 (ppm)

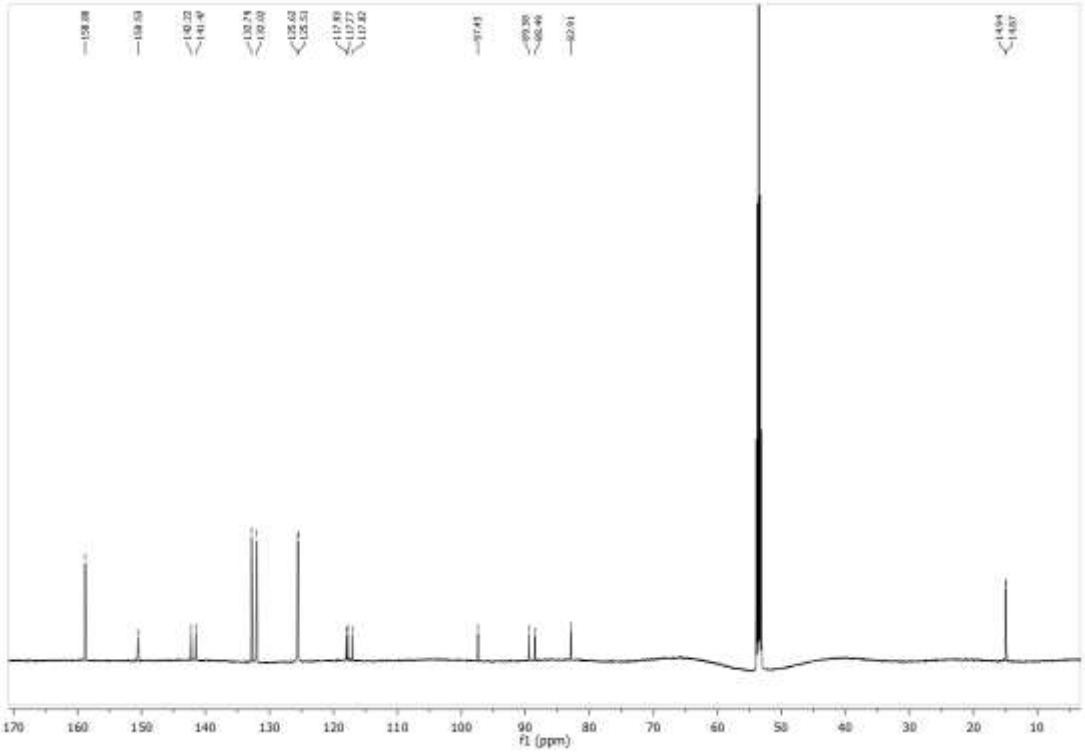
158.88
158.53
140.33
141.49
130.74
130.00
125.62
125.51
117.93
117.77
117.62
97.43
89.39
88.49
82.91
14.94
14.87
170
160
150
140
130
120
110
100
90
80
70
60
50
40
30
20
10
f1 (ppm)

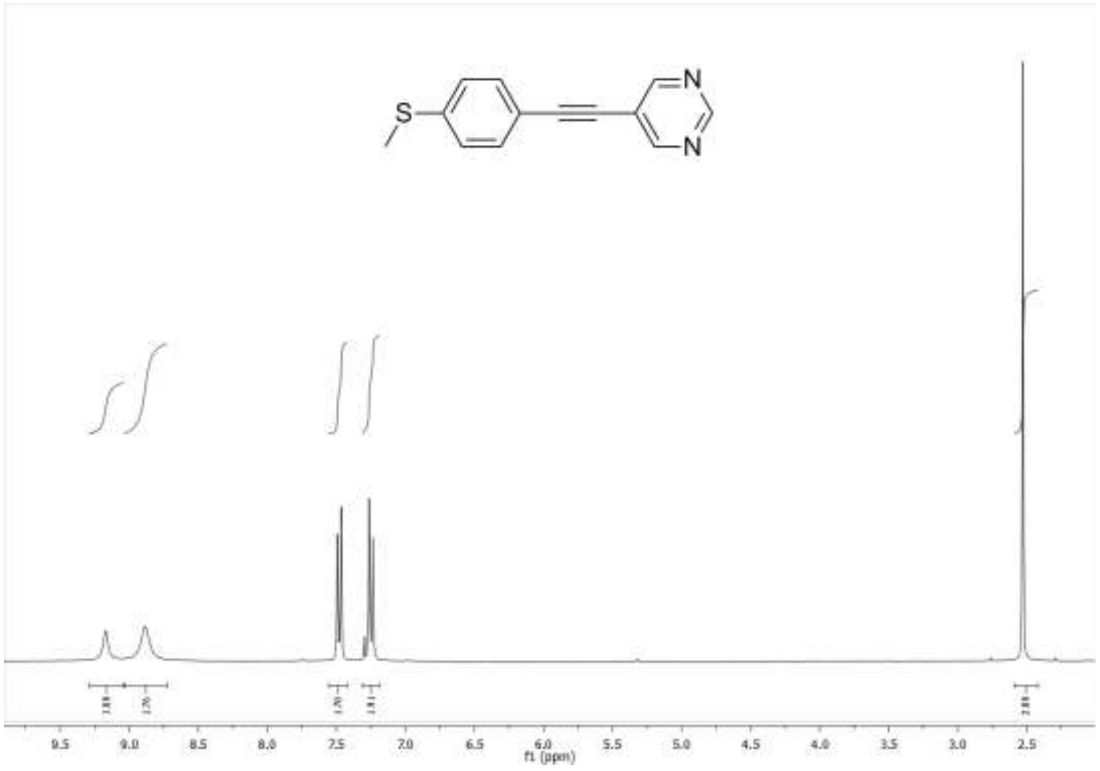
S
N
N
9.5
9.0
8.5
8.0
7.5
7.0
6.5
6.0
5.5
5.0
4.5
4.0
3.5
3.0
2.5
f1 (ppm)

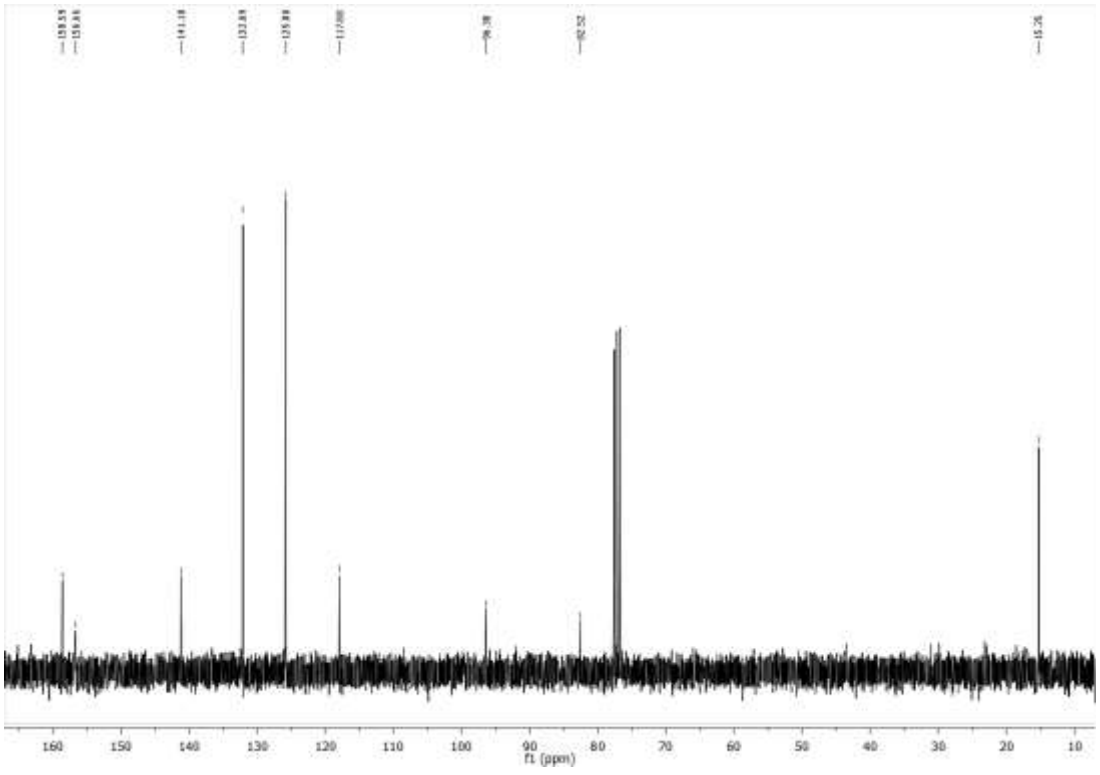
160
150
140
130
120
110
100
90
80
70
60
50
40
30
20
10
f1 (ppm)

Break junction measurements

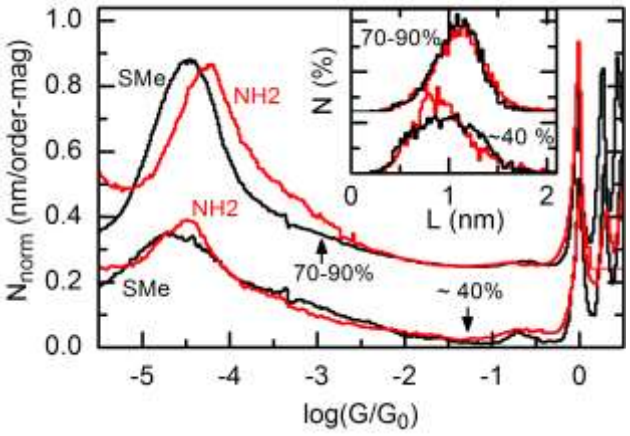

Figure S1. Comparison of the 1D conductance histograms and plateau length distributions of OPE with NH_2 and SMe as anchoring groups for 2 measurements with different percentage of traces with plateaus.[3] The figure shows that the variation observed for both anchoring groups with concentration is similar. The plateau length distribution for amines is more skewed to lower values when the concentration decreases, while starting and ending at the same length values as for SMe.

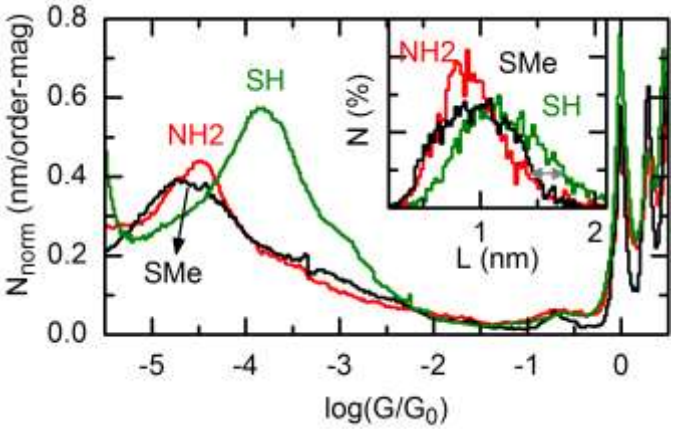

Figure S2. 1D conductance histograms for OPE with three different anchoring groups: SH, NH_2, and SMe, obtained in air after exposing a substrate to a dichlorometane solution of the compounds. The percentage of traces with plateau in these measurements were quite similar: SH: 30 ± 12 %, NH_2: 42 ± 9.0 % and SMe: 40 ± 10 %. The inset shows the plateau-length distributions. These are quite similar for SMe and NH_2, while the distribution for SH is shifted approximately 0.3 nm to higher values (indicated by the grey double arrow in the figure).

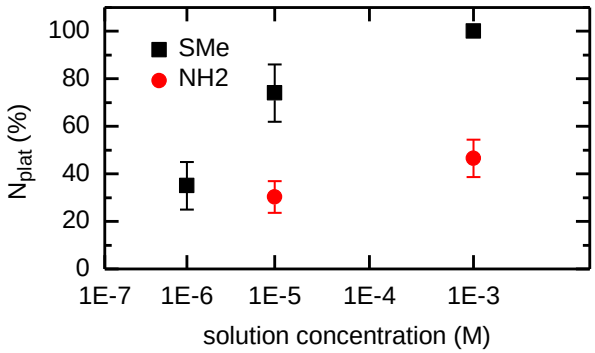

Figure S3. Percentage of traces with plateaus for different sample preparations. Here we changed the concentration of the initial solution of the compounds in CH_2Cl_2. Similar decrease in the percentage of traces with plateaus was observed by rinsing the substrates thoroughly after the exposure to a 1 mM solution (Data for NH_2 are taken from a previous communication[3]).

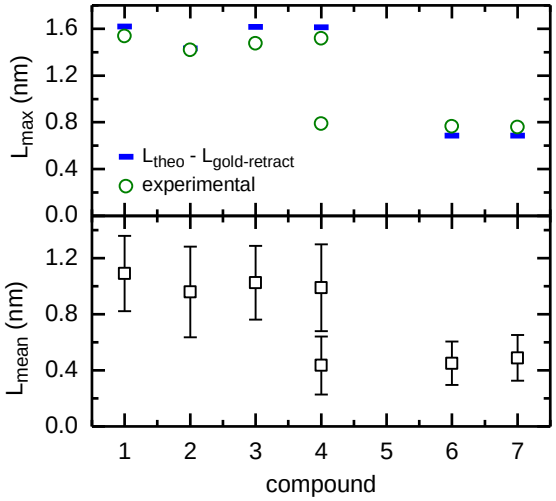

Figure S4. Mean and maximum plateau length for all the studied compounds. This are obtained from plateau-length distributions as those shown in the main text, by fitting a Gaussian curve to them. L_{mean} is the value of maximum probability, while the error bars are given by the full width at half maximum. L_{max} corresponds to the length of the longest plateaus, and is obtained as the length at which the probability decays at 15 % (2σ) of the maximum probability at the right end of the Gaussian[3]. The L_{max} values are compared with the theoretical length of each compound minus the typical gold retraction after the gold-contact breakage, which is 0.4 nm.[4] This theoretical length was calculated with hyperchem as the shortest S-S or S-N distance.

[3] Arroyo, C. R.; Leary, E.; Castellanos-Gómez, A.; Rubio-Bollinger, G.; González, M. T.; Agraït, N. *J. Am. Chem. Soc.* **2011**, *133*, 14313–14319.

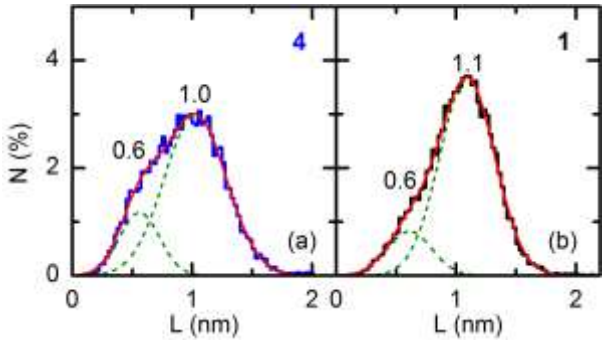

Figure S5. (a) Plateau length distribution for compound **4** obtained from all the traces with plateaus. The distribution is reproduced by the sum of two gaussians, one of them centered around 1.0 ± 0.1 nm and the other around 0.6 ± 0.02 nm. (b) Plateau length distribution for compound **1**. The peak centred at 0.6 nm has a significant lower contribution than for compound **4** to the sum of two gaussians fitting the distribution. See main text for more details.

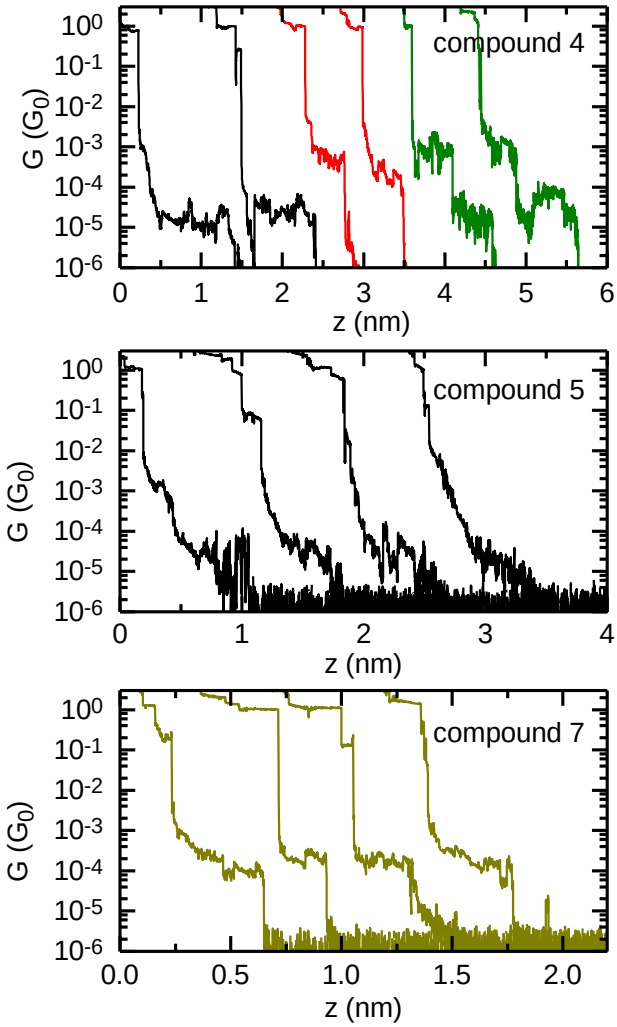

Figure S6. Individual G vs z traces for 3 of the compounds studied in this work. For compound **4**, we find traces with low conductance plateaus (2 traces at the left, black), high conductance plateaus (2 traces in the middle, red), and traces with

plateaus at high and low conductance (2 traces at the right, green). The threshold for 'high' or 'low' conductance was log(G/G0)= −3.8 (see main text for more details). For compound **5**, we do not find plateaus with clear break signalling a junction breakage, but traces with slow-decaying conductance.

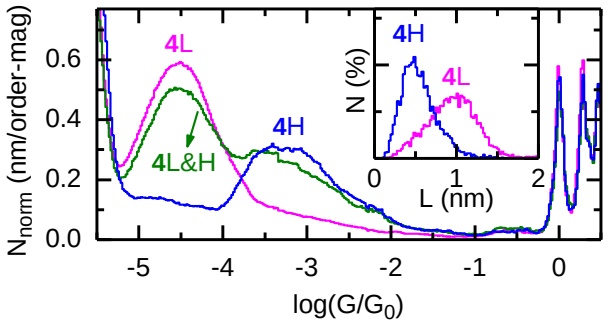

Figure S7. Resulting conductance histograms obtained after separating the traces of compound **4** in three groups: those with plateaus in the range log(G/G0)= −5.1 and −3.8 (**4H**), those with plateaus in the range log(G/G0)= −3.8 and −2 (**4L**), and those with plateaus in both previous ranges (**4L&H**). Due to the overlap in conductance values of the two peaks in the total histogram of compound **4** (Figure 3b), the separation is not clean. It does allow us to estimate the length of the high conductance plateaus, as shown in the figure inset.

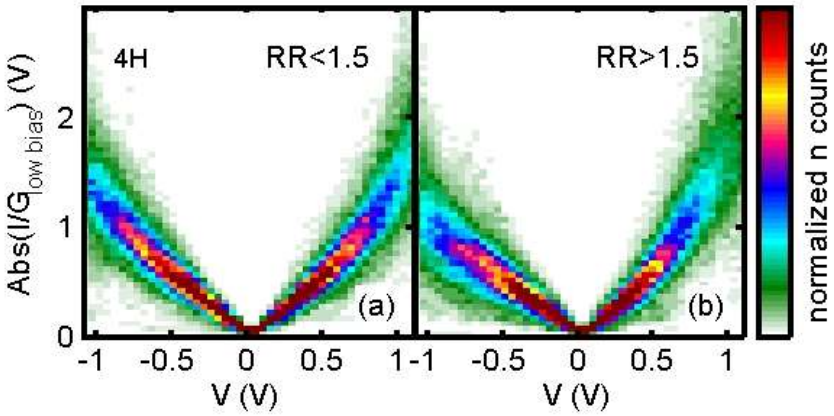

Figure S8. Two-dimensional histograms of the IV curves (normalized by the conductance close to zero bias) measured at the high conductance plateaus of compound **4** (**4**H). The IV curves have been classified into two groups according to their rectification ratio RR at ±1 V (RR=Abs[I(1V)/I(−1V)], where the higher-current branch is always the one at positive voltages): (a) includes the IV curves with RR lower than 1.5, while (b) includes those with RR larger than 1.5. The overall shape of the 2D histograms is the same for **4**L, **4**H and **7**, with quite linear IV curves. The difference among the three configurations is the percentage of measured IV curves in each group. While, for the configuration **4**L, the percentage of IV curves with RR>1.5 is around 35%, this percentage reaches 50% for **4**H, or 45% for compound **7**.

Table S1. Average of the percentage of plateaus, conductance and lengths of both high conductance and low conductance peaks observed in molecules **1**-**7**. The uncertainty in the percentages is given by the standard deviation in results from different experimental runs, while the uncertainty in the conductance values is given by the half width at half maximum of the peak in the overall histograms.

COMPOUND	% PLATEAUS	Log(G/G$_0$) High peak	Length High (nm)	Log(G/G$_0$) Low peak	Length Low (nm)	% High plateaus
1	73 ± 12			−4.5 ± 0.46	1.05 ± 0.32	8 ± 2
2	65 ± 11			−4.3 ± 0.5	0.95 ± 0.32	
3	85 ± 1.8			−4.5 ± 0.46	1.02 ± 0.26	
4	67 ± 10	−3.4 ± 0.75	0.43 ± 0.20	−4.6 ± 0.5	0.98 ± 0.34	30 ± 6
5						
6	78 ± 7.6	−3.9 ± 0.38	0.45 ± 0.16	-	-	-
7	75 ± 2.8	−3.8 ± 0.38	0.49 ± 0.16	-	-	-

Theoretical calculations.
MOLECULAR ORBITALS IN THE GAS PHASE

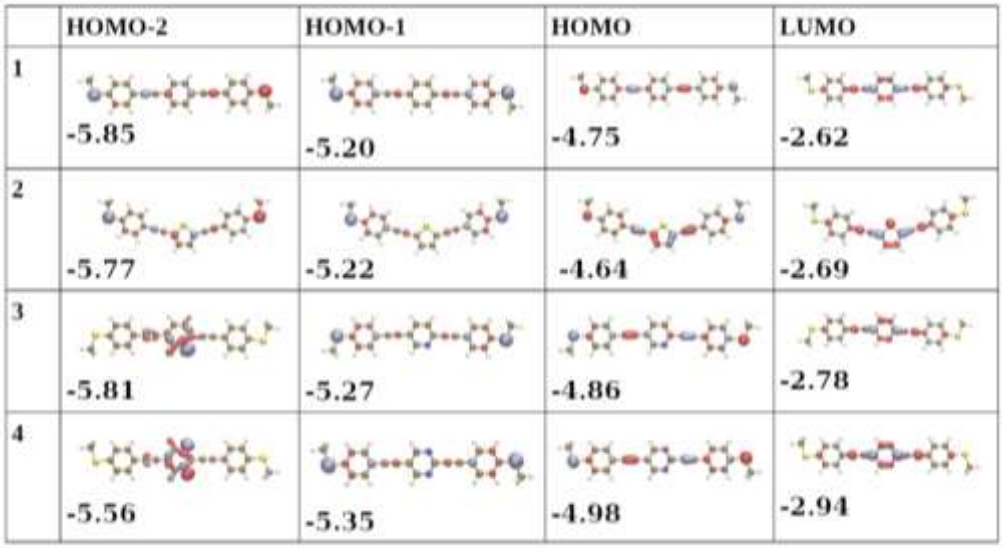

Figure S9. Molecular orbitals in the gas phase for compounds **1**-**4** and their corresponding energies (eV).

TRANSMISSION CHANNELS

In the coherent transport regime, and following the spirit of the Landauer approach, the linear conductance is given by $G = G_0 T(E_F) = G_0 \Sigma_i \tau_i(E_F)$, where $G_0 = 2e^2/h$ is the quantum of conductance , $T(E_F)$ is the junction transmission at the Fermi energy, and $\tau_i(E_F)$ are the transmission coefficients, i.e. the energy-dependent eigenvalues of the transmission matrix.

In Fig S10, we show the total transmission and the transmission coefficients for the two main channels for all molecules. It can be observed that the current mainly flows through one single channel (red dashed line), which originates from an extended orbital. Differences between the four cases are clearly visible in the transmission through a second channel (green line) which, however, does not contribute significantly to the conductance.

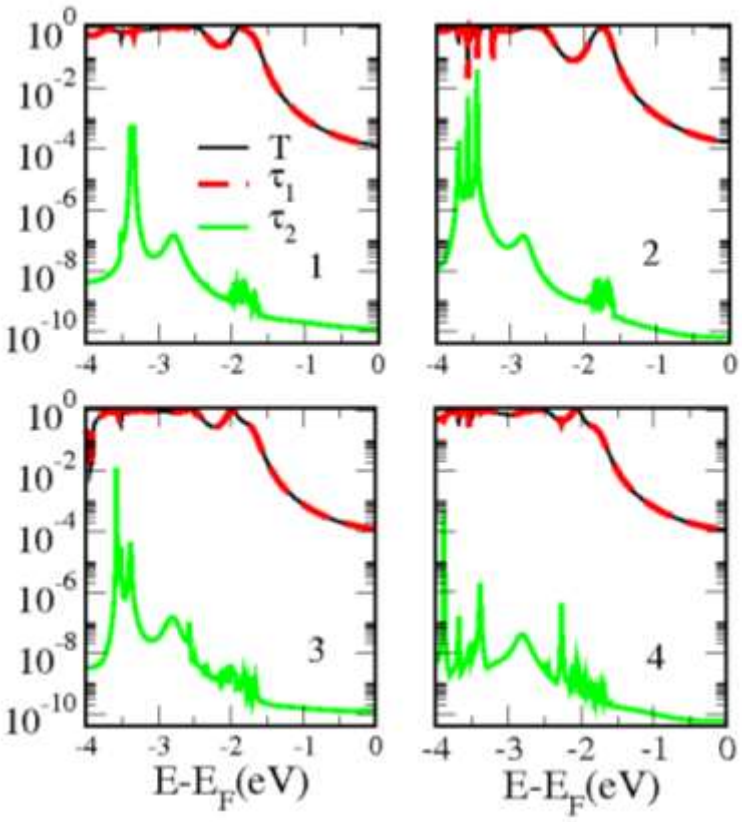

Figure S10. Total transmission T (black solid line) and individual transmission coefficients (τ_1 and τ_2) as a function of energy.

HOMO-LUMO GAP CORRECTIONS

The HOMO and all other occupied orbital energies were shifted by $\Sigma_{occ} = -IP - \varepsilon H + \Delta_{occ}$, while the LUMO and all other unoccupied orbital levels were shifted by $\Sigma_{virt} = -EA - \varepsilon L + \Delta_{virt}$. Here, Δ_{occ} (Δ_{virt}) is the image charge correction for the occupied (unoccupied) states, εH (εL) is the Kohn-Sham energy of the gas phase HOMO (LUMO), and IP (EA) is the gas phase ionization potential (electron affinity). All quantities are reported in Table S2 for all geometries.

	HOMO	IP	Δ_{occ}	LUMO	EA	Δ_{virt}
1	−4.76	−6.19	0.38	−2.64	−1.13	−0.38
2	−4.64	−6.11	0.38	−2.69	−1.14	−0.38
3	−4.87	−6.29	0.38	−2.78	−1.25	−0.38
4	−4.97	−6.40	0.39	−2.93	−1.36	−0.38
7 (b)	−5.28	−7.28	0.84	−2.76	−0.80	−1.33
7 (c)	−5.28	−7.28	0.55	−2.76	−0.80	−0.57

Table S2. : Kohn-Sham HOMO and LUMO, Ionization potential (IP), Electron affinity (EA) and image charge correction for occupied Δ_{occ} and Δ_{virt} unoccupied orbitals. All quantities are in eV.